

1 LiSc(BH₄)₄ as a Hydrogen Storage Material: Multinuclear High-Resolution Solid-State 2 NMR and First-Principles Density Functional Theory Studies

3 Chul Kim,^{†,▽} Son-Jong Hwang,^{*,†} Robert C. Bowman, Jr.,[‡] Joseph W. Reiter,[‡] Jason A. Zan,[‡]
4 James G. Kulleck,[‡] Houria Kabbour,^{§,#} E. H. Majzoub,^{||} and V. Ozolins[†]

5 Division of Chemistry and Chemical Engineering, California Institute of Technology, Pasadena, California
6 91125; Jet Propulsion Laboratory, California Institute of Technology, Pasadena, California 91109-8099;

7 Division of Engineering and Applied Science, California Institute of Technology, Pasadena, California 91125;
8 Center for Nanoscience, and Department of Physics and Astronomy, University of Missouri, St. Louis, Missouri
9 63121-4400; and Department of Materials Science and Engineering, University of California,
10 Los Angeles, California 90095-1595

11 Received: February 8, 2009; Revised Manuscript Received: April 14, 2009

12 A lithium salt of anionic scandium tetraborohydride complex, LiSc(BH₄)₄, was studied both experimentally
13 and theoretically as a potential hydrogen storage medium. Ball milling mixtures of LiBH₄ and ScCl₃ produced
14 LiCl and a unique crystalline hydride, which has been unequivocally identified via multinuclear solid-state
15 nuclear magnetic resonance (NMR) to be LiSc(BH₄)₄. Under the present reaction conditions, there was no
16 evidence for the formation of binary Sc(BH₄)₃. These observations are in agreement with our first-principles
17 calculations of the relative stabilities of these phases. A tetragonal structure in space group $I\bar{4}$ (#82) is predicted
18 to be the lowest energy state for LiSc(BH₄)₄, which does not correspond to structures obtained to date on the
19 crystalline ternary borohydride phases made by ball milling. Perhaps reaction conditions are resulting in
20 formation of other polymorphs, which should be investigated in future studies via neutron scattering on
21 deuterides. Hydrogen desorption while heating these Li–Sc–B–H materials up to 400 °C yielded only
22 amorphous phases (besides the virtually unchanged LiCl) that were determined by NMR to be primarily
23 ScB₂ and [B₁₂H₁₂]⁻² anion containing (e.g., Li₂B₁₂H₁₂) along with residual LiBH₄. Reaction of a desorbed
24 LiSc(BH₄)₄ + 4LiCl mixture (from 4LiBH₄/ScCl₃ sample) with hydrogen gas at ~70 bar resulted only in an
25 increase in the contents of Li₂B₁₂H₁₂ and LiBH₄. Full reversibility to reform the LiSc(BH₄)₄ was not found.
26 Overall, the Li–Sc–B–H system is not a favorable candidate for hydrogen storage applications.

27 I. Introduction

28 Metal borohydrides [M(BH₄)_n, M = alkali, alkali earth,
29 transition metals, etc.] have recently been extensively examined
30 for on-board hydrogen storage applications.^{1,2} While their high
31 gravimetric and volumetric capacities are appealing in view of
32 the technical targets from the US Department of Energy (DOE)³
33 for hydrogen storage in fuel cell powered vehicles, their
34 performance in reversible hydrogen storage still falls short of
35 these criteria. The hydrogen desorption temperatures, T_d , are
36 often too high, hydrogenation is irreversible or only partly
37 reversible, and the reaction kinetics are much too slow. Release
38 of diborane (B₂H₆) during the dehydrogenation process is a
39 critical issue for some materials.^{4,5} Multistep decomposition
40 sequence^{6,7} and the associated formation of numerous intermediates
41 add complexities. Various approaches have been attempted
42 in order to tackle the problems, and meaningful advances have
43 been achieved. Besides the well-known destabilization strategy,^{8,9}

44 an approach of finding an energetically favored pathway by
45 constructing proper binary systems, modifications of thermo-
46 dynamic properties were attempted by using additives,^{6,10} adding
47 halides,⁵ and use of nanoscale particles or incorporating them
48 with porous materials such as aerogels or nanotubes.^{11–14} While
49 most of these studies were concentrated on the LiBH₄ or LiBH₄/
50 MgH₂ system, survey of borohydrides with various metal
51 elements has also been attempted in the search for better
52 thermodynamic properties. The electrostatic interaction between
53 metal cation (Mⁿ⁺) and the [BH₄]⁻ complex anion was identified
54 by Nakamori et al.^{15,16} as an important factor determining the
55 stability of the metal borohydride, and the trend in the measured
56 desorption temperature T_d of different borohydrides was ratio-
57 nalized in terms of the Pauling electronegativity, χ_p , of metal
58 ions. Along this line, the idea of adjusting χ_p by employing more
59 than one metal cation, such as in MM'(BH₄)_m, has been
60 examined experimentally.¹⁷ This latter approach opens up a
61 possibility of using heavier transition metal ions, which are
62 typically not favorable because of usually low gravimetric
63 capacities. However, the potential catalytic properties of transi-
64 tion metals may also improve hydrogen storage reactivities and
65 kinetics of borohydrides. Note that the lighter Li ion can be a
66 choice for M' due to its low χ_p , and the coordination number m
67 can be varied depending on the valence state of the transition
68 metal ion M: higher values of m allow better compensation for
69 the gravimetric cost of introducing heavy transition metal ions
70 M. A proposed mechanochemical synthesis route was based on
71 the following reaction:¹⁷

* Corresponding author. E-mail: sonjong@cheme.caltech.edu.

† Division of Chemistry and Chemical Engineering, California Institute of Technology.

‡ Jet Propulsion Laboratory, California Institute of Technology.

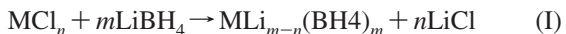
§ Division of Engineering and Applied Science, California Institute of Technology.

|| University of Missouri.

▽ University of California.

▽ Present address: Department of Chemistry, Hannam University, Dae-
jeon, S. Korea.

Present address: Unité de Catalyse et de Chimie du Solide, CNRS,
ENSC Lille, UST Lille, 59652 Villeneuve d'Ascq cedex, France.



73 Li et al.¹⁷ showed the progression of reaction I for M = Zn, Zr,
 74 Al using the formation of crystalline LiCl and changes in the
 75 Raman spectra.¹⁸ However, the formation of double-cation
 76 borohydrides has never been definitively identified or well
 77 characterized. Crystal structures of these borohydrides could not
 78 be determined from diffraction data due to loss of long-range
 79 order after the milling synthesis. A similar preparation method
 80 was claimed to form monocation borohydrides,^{15,16} so the actual
 81 identity of final products needs further investigation. Crystalline
 82 form of scandium–lithium double-cation borohydride [LiSc(BH₄)₄] was recently prepared by the same method and
 83 characterized by nuclear magnetic resonance (NMR),^{19,20} and
 84 detail structural properties were investigated by vibrational (i.e.,
 85 infrared and Raman) spectroscopy, density-functional theory
 86 (DFT) calculations, and powder X-ray diffraction.²¹ However,
 87 the dehydrogenation/hydrogenation reactions of the Li–Sc–B–H
 88 system were not examined in these studies. In the present work,
 89 we have employed multinuclear NMR and first-principles DFT
 90 calculations to elucidate the formation, structures, thermody-
 91 namic stability, and reactivity of LiSc(BH₄)₄ for potential
 92 hydrogen storage applications.

93 The mechanochemical synthesis of reaction I might provide
 94 a route for preparation of Sc(BH₄)₃ as proposed by Nakamori
 95 et al.,^{15,16} although the actual identity of the product was claimed
 96 to be LiSc(BH₄)₄ by both Hwang et al.^{19,20} and Hagemann et
 97 al.²¹ In the literature, the preparation and characterization by
 98 X-ray, IR, and solution NMR for a Sc(BH₄)₃·2THF derivative
 99 were reported,^{22–24} but, to the best of our knowledge, the
 100 isolation or characterization of pure Sc(BH₄)₃ as a solid phase
 101 has not yet been reported. The structure of the Sc(BH₄)₃
 102 compound has been predicted to be the BiI₃ type with R̄³ space
 103 group by Nakamori et al.¹⁵ In this work, we have investigated
 104 samples prepared by ball milling the mixtures of ScCl₃ and
 105 LiBH₄ with mixing ratios from 1:3 to 1:6. Combined data from
 106 high-resolution ¹¹B, ⁴⁵Sc, and ⁶Li NMR spectra and X-ray
 107 diffraction of the resulting powders were utilized for phase
 108 identifications. We have performed searches on the ground-state
 109 structures of both Sc(BH₄)₃ and LiSc(BH₄)₄ via first-principles
 110 calculations. Based on the calculated thermodynamic properties
 111 of these compounds and possible intermediates, decomposition
 112 behavior of Sc(BH₄)₃ and LiSc(BH₄)₄ with respect to hydrogen
 113 release reaction was theoretically predicted. Experimental
 114 examinations of LiSc(BH₄)₄ following hydrogen desorption/
 115 sorption treatments were also preformed.

117 II. Methods

118 **1. Theoretical Calculations.** First-principles calculations
 119 were performed with the total-energy and molecular dynamics
 120 code Vienna Ab Initio Simulation Package (VASP)^{25,26} using
 121 the generalized gradient approximation (GGA) functionals of
 122 Perdew and Wang²⁷ and Perdew–Burke–Erzenhoff (PBE)²⁸ for
 123 the electronic exchange and correlation. We adopted the
 124 projected augmented wave (PAW) approach^{28–30} to treat the
 125 interactions between the ions and valence electrons. The basis
 126 set for the electronic wave functions included plane waves below
 127 a cutoff energy of 875 eV, in conjunction with regular
 128 Monkhorst–Pack *k*-point meshes of 4×4×4 or better for all
 129 solid phases. Structural relaxations of atomic positions, cell
 130 shapes, and cell volumes were carried out until the residual
 131 forces and stresses were below 0.01 eV/Å and 0.1 GPa,
 132 respectively. The energy of the H₂ molecule was calculated in
 133 a rectangular 10 × 10 × 12 Å box. The phonon frequencies

were determined using the supercell dynamical matrix approach;
 134 the details of our method are given in ref 31.

A global optimization procedure utilizing prototype electro-
 136 static ground-state (PEGS) search³² was used to predict the
 137 currently unknown crystal structures of Sc₂(B₁₂H₁₂)₃, Sc(BH₄)₃,
 138 and LiSc(BH₄)₄. The PEGS approach determines the type and
 139 symmetry of the ground-state crystal structure by minimizing
 140 the total electrostatic energy of a collection of negatively
 141 charged, configurationally complex anions, and positively
 142 charged spherical cations, with a soft-sphere repulsion acting
 143 between overlapping ions. Monte Carlo simulated annealing in
 144 conjunction with potential energy surface smoothing techniques
 145 are used to minimize the PEGS Hamiltonian, and accurate DFT
 146 techniques are employed to calculate the total energies and fully
 147 relaxed structural parameters for the resulting minimum elec-
 148 trostatic energy structures. The PEGS search for the Sc₂(B₁₂H₁₂)₃
 149 compound used charges of +3e, 0e, and −0.1667e, for Sc, B,
 150 and H ions, respectively, resulting in a total charge of −2e on
 151 the B₁₂H₁₂ icosahedral anion. The [B₁₂H₁₂]^{2−} anion was modeled
 152 as rigid icosahedron with a center to vertex distance of 1.43 Å,
 153 with (exterior) hydrogen atoms of radius of either 1.3 or 1.43
 154 Å at each of the 12 vertex positions. The Sc radius was set at
 155 0.75 Å. PEGS runs using a hydrogen radius of 1.43 Å produced
 156 structures with lower energies and higher symmetries. For
 157 LiSc(BH₄)₄ and Sc(BH₄)₃, ionic charges of +1e, +3e, 0e, and
 158 −0.25e were used for Li, Sc, B, and H ions, respectively. Ionic
 159 radii were 0.68, 0.75, and 1.3 Å for Li, Sc, and H, respectively.
 160 The [BH₄][−] anion was modeled as a rigid tetrahedral molecule
 161 with a B–H bond length of 1.23 Å.

Equilibrium phase diagrams and thermodynamically revers-
 163ible hydrogen storage reactions in the Li–Sc–B–H system were
 164 determined using the grand canonical linear programming
 165 (GCLP) method proposed in ref 33. The following solid-state
 166 phases were included in our study: B, Li, LiBH₄, Li₂B₁₂H₁₂,
 167 LiH, LiSc(BH₄)₄, Sc, ScB₂, ScB₁₂, Sc(BH₄)₃, Sc₂(B₁₂H₁₂)₃, and
 168 ScH₂.

2. Experimental Section. The synthesis of scandium/lithium
 170 borohydride was achieved using the ball-milling technique with
 171 different ratios of ScCl₃ and LiBH₄. Anhydrous ScCl₃ (Alfa
 172 Aesar, 99.9%) and LiBH₄ (Aldrich, ≥90%) were used without
 173 further purification. These reactants were mixed together in an
 174 Ar-filled glovebox and placed in an 80 mL rubber gasket sealed
 175 steel vessel, with five 0.5 in. diameter steel balls. The argon-
 176 filled vessel was then placed in a Fritsch Pulverizette 6 planetary
 177 mill. The mixture was subsequently milled at 500 rpm for 3 h.
 178 Hydrogen desorption was performed at a temperature of 400
 179 °C in an initially evacuated volume to a pressure between 1
 180 and 3 atm of H₂ gas in a stainless-steel reactor vessel that was
 181 described previously.³⁴ Hydrogen absorption was performed at
 182 a temperature of 400 °C and a pressure of 70 bar of H₂ gas.

Solid-state MAS NMR measurements were performed using
 184 a Bruker Avance 500 MHz spectrometer equipped with a Bruker
 185 4 mm CPMAS “boron-free” probe. MAS NMR samples were
 186 loaded in a 4 mm ZrO₂ rotor and sealed with a tightly fitting
 187 Kel-F cap inside a glovebox in order to avoid any contact with
 188 air or moisture. The spectral frequencies were 500.23, 160.50,
 189 73.61, and 121.53 MHz for ¹H, ¹¹B, ⁶Li, and ⁴⁵Sc nuclei,
 190 respectively. A typical MAS spectrum of a quadrupole nucleus
 191 was recorded at a MAS spinning rate of 10–13 kHz applying
 192 two-pulse phase modulation (TPPM)³⁵ ¹H decoupling pulse
 193 scheme after a short (0.3–0.5 μs) single pulse (i.e., <π/12 for
 194 ¹¹B) at room temperature. Dried N₂ gas was used for spinning.
 195 CPMAS spectra for ¹¹B[¹H] were obtained with the cross-
 196 polarization mixing times of 50 μs to 1 ms in the sudden passage

TABLE 1: Two Possible Reaction Routes during the Ball-Milling Process

ratio	nonionic route	ionic route
1:3	$\text{ScCl}_3 + 3\text{LiBH}_4 \rightarrow \text{Sc}(\text{BH}_4)_3 + 3\text{LiCl}$	$\text{ScCl}_3 + 3\text{LiBH}_4 \rightarrow 3/4\text{LiSc}(\text{BH}_4)_4 + 9/4\text{LiCl} + 1/4\text{ScCl}_3$
1:4	$\text{ScCl}_3 + 4\text{LiBH}_4 \rightarrow \text{Sc}(\text{BH}_4)_3 + 3\text{LiCl} + \text{LiBH}_4$	$\text{ScCl}_3 + 4\text{LiBH}_4 \rightarrow \text{LiSc}(\text{BH}_4)_4 + 3\text{LiCl}$
1:6	$\text{ScCl}_3 + 6\text{LiBH}_4 \rightarrow \text{Sc}(\text{BH}_4)_3 + 3\text{LiCl} + 3\text{LiBH}_4$	$\text{ScCl}_3 + 6\text{LiBH}_4 \rightarrow \text{LiSc}(\text{BH}_4)_4 + 3\text{LiCl} + 2\text{LiBH}_4$

regime by use of low rf fields.^{19,36,37} NMR shifts were externally referenced to TMS, BF₃•O(CH₂CH₃)₂, 1 M LiCl aqueous solution, and Sc(NO₃)₃ aqueous solution at 0 ppm for the ¹H, ¹¹B, ⁶Li, and ⁴⁵Sc nuclei, respectively.

The XRD measurements were performed at room temperature on a Siemens D500 diffractometer operating with Cu K α radiation. Each Li–Sc–B–H XRD sample used a small amount of NIST-traceable silicon (Si) powder as an internal standard for locating peak positions. The powders were placed on a XRD cell between two Kapton films to reduce scattering background while protecting the samples from air exposure and the loaded cells were stored under argon until the XRD measurements were performed.

III. Results and Discussion

III.A. Preparation of Scandium Borohydride: LiSc(BH₄)₄ vs Sc(BH₄)₃. Solid-phase products from the mechanochemical synthesis of $\text{ScCl}_3 + n\text{LiBH}_4$ (see reaction I) were analyzed for the presence of two possible compounds: LiSc(BH₄)₄ and Sc(BH₄)₃. Sc(BH₄)₃ is a neutral scandium complex and represents a monocation borohydride. We label this reaction pathway the “nonionic route”. On the contrary, LiSc(BH₄)₄ is a lithium salt of an anionic scandium complex, a double-cation borohydride, and we label this the “ionic route”. Regardless of the molar ratio n between the two starting reactants, we believe that thermodynamics controls these reactions and simultaneous formation of LiSc(BH₄)₄ and Sc(BH₄)₃ is unlikely. Since the reference materials of Sc(BH₄)₃ or LiSc(BH₄)₄ are unavailable for spectroscopic comparison, our approach in the analysis was to quantitatively measure identifiable chemical compounds in a ball milled mixture. The strategy appears to be a good choice because variation of the molar ratio n diversifies kinds of chemical species and their ratios among reactants and products as listed in Table 1. The distribution certainly differs depending on the reaction pathway. For example, the reaction equations for the case of $n = 4$ (see Table 1) shows 3:1 ratio between LiCl and LiBH₄ for the nonionic route while it is 3:0 for the ionic route (no LiBH₄ left). The ratio of two compounds can be readily measured spectroscopically. In this way, indirect evidence of the reaction pathway could be obtained under the circumstance of unavailable Sc(BH₄)₃ and LiSc(BH₄)₄ compounds. We have prepared three samples with $n = 3, 4, 6$, and the quantitative measurement was performed by multinuclear solid-state NMR. Besides the appearance of diffraction peaks attributable to LiCl in the XRD patterns shown in Figure 1, additional peaks were seen from all three samples to be a signature of a newly formed compound with moderate crystallinity (250–300 Å). The formation of LiCl by itself was not useful in determining the reaction route. The XRD patterns in Figure 1 also clearly show that a single new phase was formed independent of the LiBH₄ to ScCl₃ ratio, n . We have found that indexing of the XRD peaks in Figure 1 (excluding LiCl peaks) leads to reasonable agreement with tetragonal structures with space groups P4 (#75), I4cm (#108), P4₂mmc (#131), and P4₂c (#112) which was specified in the report by Hagemann et al.²¹

We also found that an orthorhombic structure Pbam (#55) with lattice parameters $a = 0.608$ nm, $b = 1.211$ nm, and $c = 0.604$ nm showed a reasonable indexing agreement. However, the

signal-to-noise and resolution problems in our present XRD data provoke ambiguities that prevent a better analysis, and it appeared that a reasonably good match could be found with the space group P4₂c as shown in Figure 1B. Therefore, we can conclude that our room temperature crystal structure of our LiSc(BH₄)₄ compounds, formed with three different molar ratio $n (=3, 4, 6)$, is in good agreement with the previous report.²¹ It is noteworthy that although some LiBH₄ is detected by XRD for the 6:1 sample, no peaks from ScCl₃ or other possible compounds can be seen in Figure 1.

Multinuclear MAS NMR spectra of three solid-phase products are shown in Figures 2 and 3. ¹¹B and ⁴⁵Sc spectra of starting materials LiBH₄ and ScCl₃ are also included for comparison in Figure 2, and so are our measured ⁶Li NMR spectra of LiBH₄ and LiCl in Figure 3. At the first glance, the mechanochemical reactions appear to proceed with the disappearance of the LiBH₄ peaks from ¹¹B (-41 ppm) and ⁶Li (-1.2 ppm) MAS NMR. Decomposition of ScCl₃ and new scandium compound formation

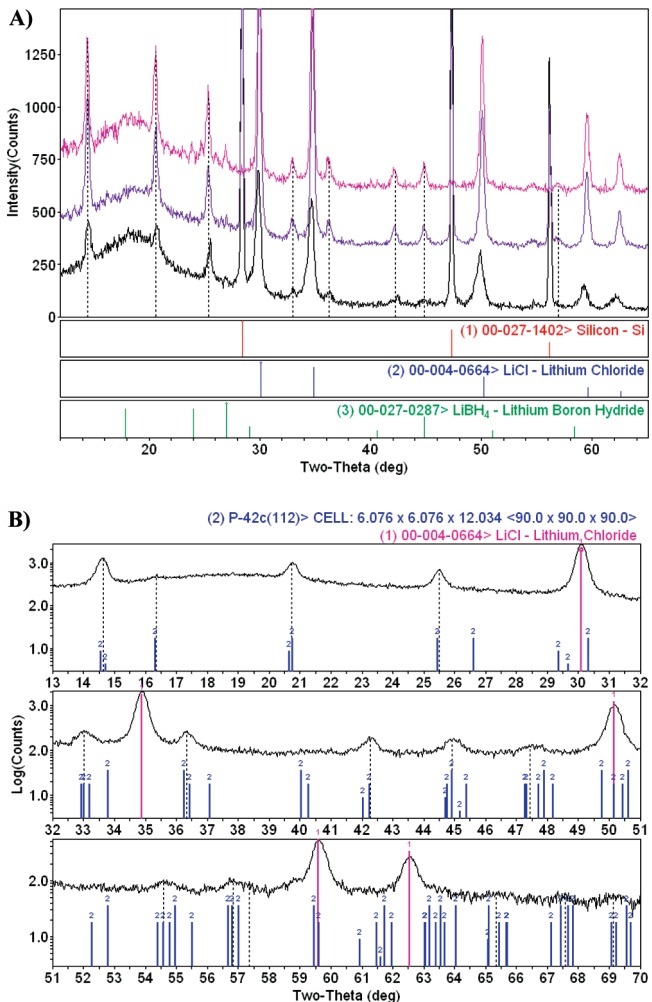


Figure 1. (A) Powder X-ray diffraction profiles of ball-milled $\text{ScCl}_3 + n\text{LiBH}_4$ samples (top is $n = 6$, middle is $n = 4$, and bottom is $n = 3$) plus silicon (Si) added as an internal reference. (B) Comparison of XRD profile of ball-milled $\text{ScCl}_3 + 4\text{LiBH}_4$ sample with $P4_2c$ of Hagemann et al.²¹

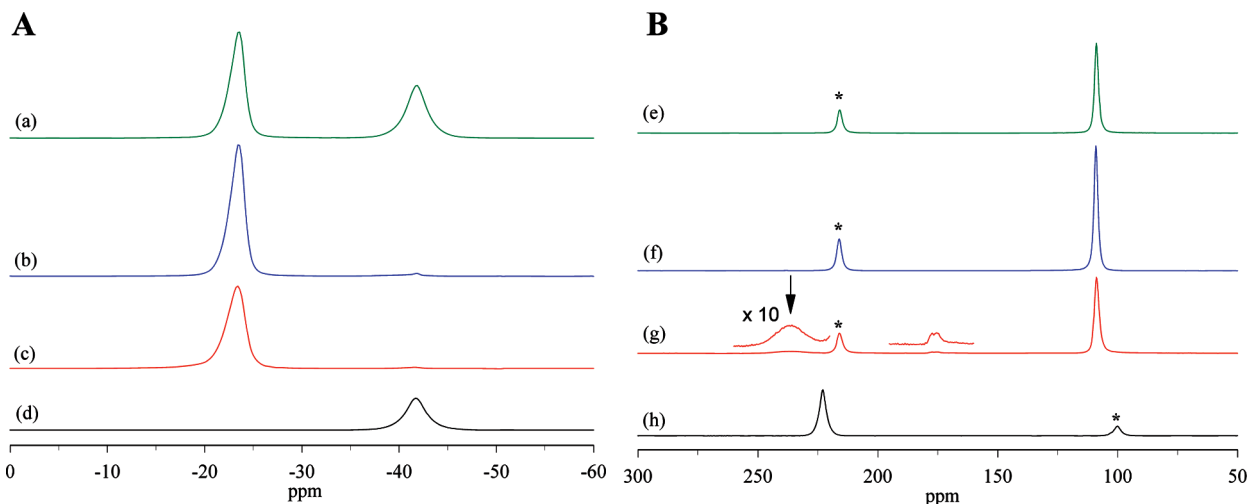


Figure 2. (A) (a–d) ^{11}B MAS NMR; (B) (e–h) ^{45}Sc MAS NMR spectra of the ball-milled $\text{ScCl}_3 + n\text{LiBH}_4$: (a,e) $n = 6$, (b,f) $n = 4$, (c,g) $n = 3$, and (d) LiBH_4 , (h) ScCl_3 . Note that parts of (g) were overlaid with higher vertical scale ($\times 10$) (see arrow) in order to show the presence of 240 and 175 ppm peaks. Referencing to ScCl_3 aqueous solution for ^{45}Sc NMR is possible by adding +4.8 ppm to the current chemical shift scale. The asterisks indicate spinning sidebands.

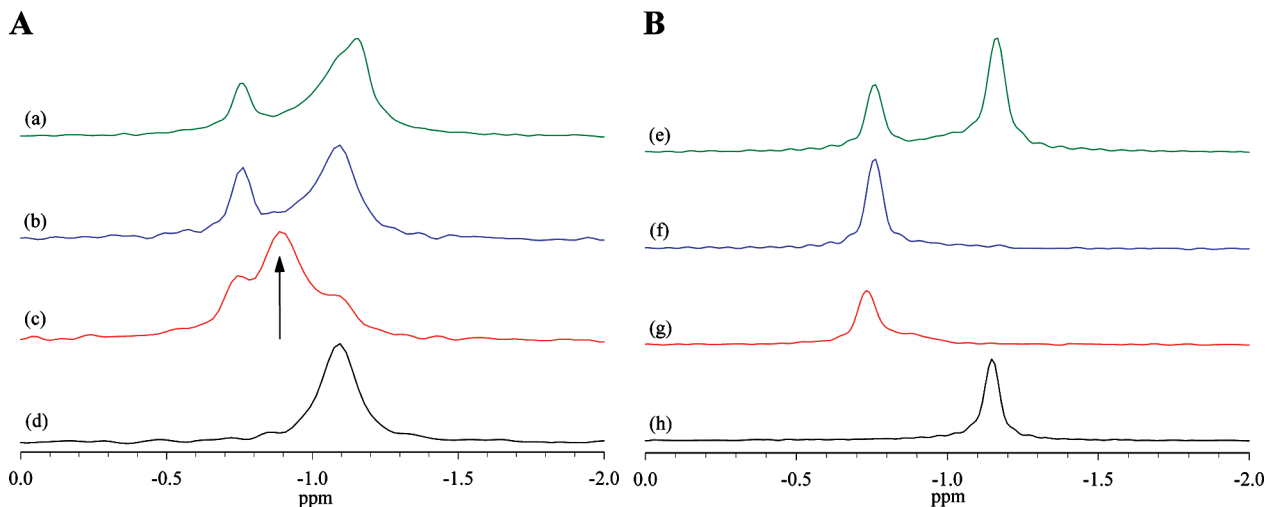


Figure 3. ^6Li MAS (a–d) and CPMAS (e–h) NMR spectra of the ball-milled $\text{ScCl}_3 + n\text{LiBH}_4$: (a,e) $n = 6$, (b,f) $n = 4$, (c,g) $n = 3$, and (d) LiCl , (h) LiBH_4 . The arrowed peak does not correspond to a hydride phase.

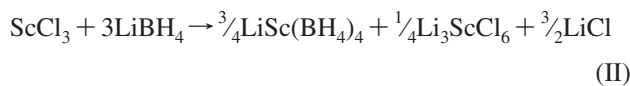
are also clear from ^{45}Sc NMR. The primary new compound formed by ball-milling is characterized by NMR signatures appearing at -23 , 108.5 , and -0.7 ppm for ^{11}B , ^{45}Sc , and ^6Li nuclei, respectively. Although some changes were observed from the proton (^1H) MAS NMR spectra, it was not possible to assign any of the unresolved components to specific hydrides. Without knowing the identity of the resulting compound, there are a number of observations in the NMR results that allow us to identify the reaction route. These include the following: (i) ^{11}B MAS NMR indicated unreacted LiBH_4 only when $n = 6$ (i.e., 1:6 ratio), which agrees with the XRD results in Figure 1. (ii) The integral ratio of ^{11}B peaks at -41 ppm (LiBH_4) and -23 ppm (initially unassigned) in the 1:6 ratio sample was about 2, as was expected in the Ionic route in Table 1. Note that the molar ratio between $\text{Sc}(\text{BH}_4)_3$ and LiBH_4 in the Nonionic route is expected to be 1:3 (see Table 1) for this mixing ratio. (iii) Besides the 108.5 ppm peak of new product, excess ScCl_3 is likely visible but as a broad peak at 237 ppm in ^{45}Sc NMR spectrum shown in Figure 2g found for $n = 3$, as was predicted from the ionic route. We will show shortly the broadening and slight upfield shift in chemical shift is most likely associated with a further reaction of ScCl_3 with the LiCl that was formed during ball milling. (iv) ^6Li MAS NMR identifies the presence

of LiCl (-1.1 ppm) and LiBH_4 (-1.2 ppm) in addition to the peak of the product at -0.7 ppm. The absence of LiBH_4 is clear for the 1:4 sample. The integration of the ^6Li peaks yielded the relative intensity ratio of about 1:3:2 for the 1:6 ratio sample, as evident for the ionic route in Table 1. Note that the quantitation proceeded with additional caution due to the fact that ^6Li nuclei tend to give rise to very long relaxation time (T_1). The recycle delay time for typical ^6Li MAS NMR was 2000 s and delay times over 20 000 s were often examined to make sure full recovery of the ^6Li NMR signal. All these results consistently support the ionic route as the reaction pathway in our ball-milling synthesis. For three different cases, the reactions appear to be completed within our ball-milling synthesis condition (i.e., 500 rpm for 3 h). Therefore, we believe it is reasonable to conclude that the reaction product must be $\text{LiSc}(\text{BH}_4)_4$, a double-cation borohydride and not $\text{Sc}(\text{BH}_4)_3$ as suggested by Nakamori et al.^{15,16,18} Consequently, the NMR signatures can be assigned to $\text{LiSc}(\text{BH}_4)_4$: -23.0 ppm for ^{11}B , 108.5 ppm for ^{45}Sc , and -0.7 ppm for ^6Li . More detailed NMR characterization of $\text{LiSc}(\text{BH}_4)_4$ will be presented shortly.

Some additional observations were made from ^6Li and ^{45}Sc NMR of the 1:3 sample. In addition to the two anticipated compounds, $\text{LiSc}(\text{BH}_4)_4$ and LiCl supposedly with a 1:3 ratio

LiSc(BH₄)₄ as a Hydrogen Storage Material

according to Table 1, the ⁶Li spectrum shows a strong peak at -0.9 ppm (see Figure 3c). The intensity ratio between LiSc(BH₄)₄ and LiCl definitely deviates from the expected ratio. From the deconvolution of this spectrum (not shown), we found a 1:2:1 ratio describes the distribution of lithium ions of LiSc(BH₄)₄ (-0.7 ppm): unknown (-0.9 ppm): LiCl (-1.1 ppm), instead of a 1:3 ratio for LiSc(BH₄)₄ (-0.7 ppm) to LiCl. This indicates that a new lithium compound was formed as a result of LiCl reacting with residual ScCl₃. From the reaction equation in Table 1 and the lithium quantitation by ⁶Li MAS NMR, it is possible to conclude that a complex with [(1/4)(6LiCl•ScCl₃] composition might be formed, and the -0.9 ppm peak is responsible for the unknown species. To our best knowledge, Li–Sc–Cl complex with such ratio has not been reported previously. For the case of possible formation of a known ternary Li₃ScCl₆ compound,³⁸ a modified reaction equation could be proposed as follows:



336

However, the expected Li ratios of 1:1:2 are inconsistent with the present observed ratio found by quantitative analysis of the ⁶Li MAS NMR spectrum in Figure 3c. We could not detect the Li₃ScCl₆ compound by XRD, and we also could not find any reported MAS NMR results in the literature to confirm the formation of Li₃ScCl₆ based on ⁶Li and ⁴⁵Sc peaks. As mentioned previously, ⁴⁵Sc MAS NMR results for this 1:3 sample also indicated that the bonding and coordination geometry around scandium cation reveals subtle changes from pure ScCl₃ (see Figure 2g with both the peak near 240 ppm marked by an arrow and a smaller peak with a shift near 175 ppm that is visible upon signal enhancement). Since neither of these peaks were obtained during ⁴⁵Sc{¹H} CPMAS experiments (spectra not shown here) while the 108.5 ppm peak from LiSc(BH₄)₄ was present, it is certain that these Sc species are not associated with the [BH₄]⁻ units. Note that there is no indication for presence of other species in ¹¹B MAS NMR (see Figure 2c). In addition, the proximity between Li ion and [BH₄]⁻ was probed by employing ⁶Li{¹H} CPMAS NMR method that utilizes magnetic spin polarization of abundant nuclei (i.e., ¹H) to indirectly detect rare nuclei (i.e., ⁶Li). In such way, the discrimination of lithium nuclei in a complex with [BH₄]⁻ unit versus nonprotonated elements (i.e., LiCl or ScCl₃) is possible. The ⁶Li CPMAS NMR spectra are presented in Figure 3B for the same series of samples used for ⁶Li MAS NMR in Figure 3A. The presence of LiCl is nicely filtered out in CPMAS NMR spectra while LiBH₄ and LiSc(BH₄)₄ are seen in Figure 3B, demonstrating the value of CP method to discriminate between phases with or without hydride units. It is noteworthy that the separation of LiCl and LiBH₄ resonances exhibits only a ~ 0.1 ppm difference in ⁶Li chemical shift, which would be impossible without the support of the CP method and the very narrow lines for this nucleus. The ⁷Li NMR spectra cannot be used to distinguish between these species due to their much broader lines that hinder the resolution.^{20,39} From the fact that the -0.9 ppm peak is not detected in ⁶Li CPMAS NMR of the 1:3 sample, we eliminated the possibility of the ⁶Li peak at -0.9 ppm in spectrum Figure 3c as being associated with either of the borohydride phases.

III.B. Crystal Structures. 1. Crystal Structure of LiSc(BH₄)₄. While the synthesis of new chemical species LiSc(BH₄)₄ was confirmed by NMR in the previous section, the long-range order structure of the compound remains unsolved.

J. Phys. Chem. C, Vol. xxx, No. xx, XXXX E

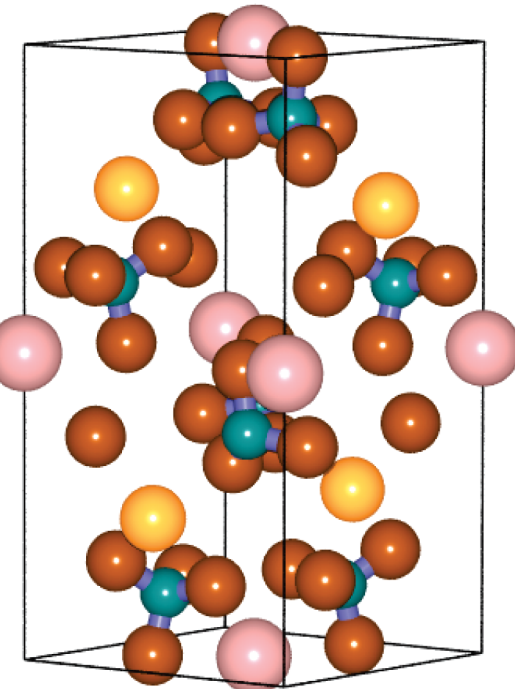


Figure 4. Tetragonal structure for LiSc(BH₄)₄ in space group $\bar{I}4$ (#82). Li (Sc) atoms are colored gold (rose).

Hagemann et al.²¹ recently reported a crystal structure for LiSc(BH₄)₄ produced using a similar mechanochemical synthesis method and proposed a $P\bar{4}2c$ space group using high-resolution synchrotron X-ray powder diffraction. We have carried out prototype electrostatic ground state (PEGS) search and first-principles DFT calculations to predict the $T = 0$ K ground-state crystal structure of LiSc(BH₄)₄. Our findings are summarized in Table 3, which lists the total energies relative to the lowest-energy structure found in the present study. In addition to PEGS, we performed a LiSc(BH₄)₄ crystal structure search using known prototype ABC₄X₁₆ compounds from the Inorganic Crystal Structure Database (ICSD). An ICSD search using the formula ABC₄X₁₆ produces two prototype CuU(MoO₄)₄ structures in space groups $\bar{P}1$ (#2), and $P2/c$ (#13). Ambiguity between the A and B sites for Li and Sc occupations was resolved by relaxing these structures with Li on A and Sc on B, and again with Li and Sc positions reversed. Only the lowest energy structures for each prototype are shown in Table 3. The PEGS search produces a low-energy structure with symmetry $\bar{I}4$ (#82). The LiSc(BH₄)₄ structure with the lowest energy and highest symmetry is the PEGS predicted $\bar{I}4$ structure, which is shown in Figure 4. First-principles DFT calculations of the phonon spectrum of $\bar{I}4$ using both two- (44 atoms) and four-formula unit supercells (88 atoms) indicate that the PEGS $\bar{I}4$ crystal structure is dynamically stable. Li and Sc atoms are 4-fold coordinated with [BH₄]⁻ anions. Each anion is oriented with three H atoms equidistant from the Sc, and the fourth H atom in the direction directly opposite the Sc. The [BH₄]⁻ anions are oriented with two H atoms (forming a tetrahedral edge) toward each Li atom. This highly symmetrical arrangement is not observed in the $P\bar{4}2c$ structure discussed below. Nearest-neighbor distances for the $\bar{I}4$ structure are shown in Table 2. The Li–H and Sc–H distances are in agreement with those in LiH (2.04 Å)⁴⁰ and ScH₂ (2.07 Å),⁴¹ respectively.

Note that our limited XRD data supports the space group $P\bar{4}2c$ (#112) that has been suggested by Hagemann et al.²¹

381
382
383
384
385
386
387
388
389
390
391
392
393
394
395
396
397
398
399
400
401
402
403 F4
404
405
406
407
408
409
410
411
412
413
414 T2
415
416 T3
417
418

TABLE 2: Nearest-Neighbor Distances (Å) in the PEGS Predicted LiSc(BH₄)₄ Structure in Space Group $\bar{I}4$

H–H	1.98	B–B	3.72
H–Li	2.00	Sc–H	2.15
Li–Li	6.48	Sc–Li	4.42
B–H	1.21	Sc–B	2.32
B–Li	2.50	Sc–Sc	6.48

TABLE 3: Relative Stability of Competing Structures for LiSc(BH₄)₄ Calculated Using First-Principles DFT at T = 0 K

structure type	symmetry	space group no.	E – E ₀ (kJ/mol fu) ^a	density (g/cm ³)
PEGS	$\bar{I}4$	82	0.0	0.743
2×1×1 Li 4k	P222 ₁	17	39	0.841
1×1×1 Li 2e	P42c	112	62	0.792
CuU(MoO ₄) ₄	P $\bar{1}$	2	138	0.720
CuU(MoO ₄) ₄	P2/c	13	315	0.888

^a Energy units are kJ/mol formula unit.

TABLE 4: Wyckoff Positions for Two Structures of LiSc(BH₄)₄, in Space Groups P42c (#112) and $\bar{I}4$ (#82)

atom	Wyckoff position	X	Y	Z
$\bar{P}42c$, a = 6.076 Å, c = 12.034 Å				
Li (0.5 occ)	4k	0	0	0.104
Sc	2c	1/2	1/2	1/4
B	8n	0.7500	0.6722	0.6386
H	8n	0.7939	0.6688	0.7251
H	8n	0.8960	0.6926	0.5891
H	8n	0.6394	0.8072	0.6234
H	8n	0.6705	0.5201	0.6166
$\bar{I}4$, a = 6.479 Å, c = 12.043 Å				
Li	2c	0	0.5000	0.2500
Sc	2b	0	0	0.5000
B	8g	0.3534	0.2469	0.8889
H	8g	0.7621	0.6206	0.3339
H	8g	0.5416	0.2551	0.8711
H	8g	0.2852	0.4221	0.8705
H	8g	0.3325	0.2111	0.9890

419 from their Rietveld refinement of X-ray synchrotron data.
 420 This $\bar{P}42c$ structure places the Li ion in a 4k site (see Table
 421 4 for atomic positions), requiring half-occupancy to obtain
 422 the correct stoichiometry. As stated in ref 21, the (Rietveld)
 423 refinement of the Li position started at (0,0,0), with a
 424 Wyckoff designation of 2e, and was allowed to move to
 425 (0,0,0.104), increasing the site multiplicity by a factor of 2,
 426 and requiring the occupancy to be reduced to 0.5. First-
 427 principles DFT was used to investigate both the idealized
 428 structure with Li at the 2e site, and the structure with Li on
 429 the 4k site at half-occupancy. Frozen phonon calculations
 430 using a 1×1×1 supercell of $\bar{P}42c$ with Li on the 2e site at
 431 full occupancy indicate a dynamically unstable structure with
 432 more than 10 imaginary frequency modes. In order to
 433 investigate the structure using the half-occupancy 4k Li atom
 434 positions, a 2×1×1 supercell was built from the $\bar{P}42c$
 435 structure, with Li at (0,0,0.104) and having the correct
 436 stoichiometry by the following method. The 1×1×1 structure
 437 was doubled along the x-axis. The Li ion positions in the
 438 left (right) half were obtained by taking the two 2e sites and
 439 moving their fractional coordinates up (down) in z by 0.104.
 440 In the resulting 2×1×1 supercell (with symmetry P222₁),
 441 the fractional coordinates of the Li were (0,0,0.104),
 442 (0,0,0.604), (0.5,0,0.396), and (0.5,0,0.896). A first-principles
 443 relaxation of the atomic coordinates and lattice parameters
 444 of this structure results in significant reorientation of the BH₄

TABLE 5: Relative Stability of Competing Structures for Sc(BH₄)₃ Calculated Using First-Principles DFT at T = 0 K

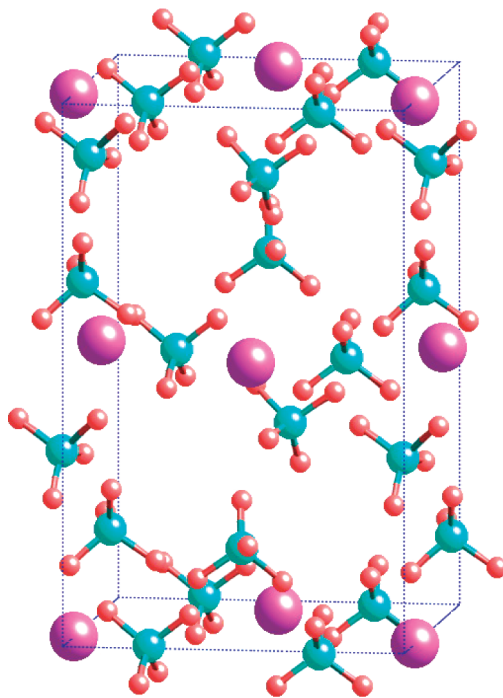
structure type	symmetry	space group no.	E – E ₀ (kJ/mol fu) ^a	density (g/cm ³)
PEGS	C222 ₁	20	0.0	0.722
La(AuF ₄) ₃	R3-c	167	10.7	1.061
Lu(ClO ₄) ₃	R3c	161	10.7	1.061
Nd(AlBr ₄) ₃	P3 ₁ 21	152	16.7	0.716
Y(AlCl ₄) ₃	P3 ₁ 12	151	18.3	0.648
BiI ₃ (ref. [15])	R $\bar{3}$	148	44.1	0.924
Nd(ClO ₄) ₃	P6 ₃ /m	176	164.5	1.203

^a Energy units are kJ/mol formula unit.

anions and lowering of the total energy by 21 kJ/mol fu. While the cell symmetry remains in P222₁ (#17), there is a significant increase in the density from 0.792 to 0.841 g/cm³. The (T = 0 K) energies of both the 1×1×1 P42c structure with idealized Li positions, and the 2×1×1 P222₁ structure remain well above the PEGS $\bar{I}4$ structure, as shown in Table 3. Calculated diffraction peak positions from the PEGS $\bar{I}4$ structure are not in agreement with the experimental pattern. This indicates two possibilities. Either PEGS has generated a polymorph of the LiSc(BH₄)₄ structure which is not the ground state, or the actual ground-state structure is $\bar{I}4$, but is inaccessible via ball milling. We note that while the fit to the diffraction data in Hagemann et al.²¹ is compelling, our results suggest that further studies are needed to clarify the crystal structure(s) of LiSc(BH₄)₄. In particular, neutron diffraction measurements should be done on appropriately isotope labeled deuterated samples. It may be possible to perform annealing studies of the product LiSc(BH₄)₄ under hydrogen pressure to access the $I4$ phase, or even observe a range of polymorphs as a function of temperature, as is observed⁴² in Ca(BH₄)₄.

2. Crystal Structure of Sc(BH₄)₃. An earlier theoretical study by Nakamori et al.¹⁵ suggested that Sc(BH₄)₃ would adopt a trigonal structure of R3 symmetry, which was derived from the structure adopted by the binary BiI₃ compound. We performed both PEGS and ICSD searches based on the AB₃X₁₂ structure type. The results of these searches are summarized in Table 5. The following structure types were taken from the International Crystal Structure Database: Nd(ClO₄)₃, Pr(ClO₄)₃, Eu(ClO₄)₃, and Yb(ClO₄)₃ in space group P6₃/m (#176); Tb(AlCl₄)₃, Y(AlCl₄)₃, Dy(AlCl₄)₃, and Ho(AlCl₄)₃ in space group P3₁12 (#151); Yb(ClO₄)₃ and Lu(ClO₄)₃ in space group R3c (#161); La(AuF₄)₃ in space group R3-c (#167); Nd(AlBr₄)₃, Pr(AlBr₄)₃, and La(AlBr₄)₃ in space group P3₁21 (#152).

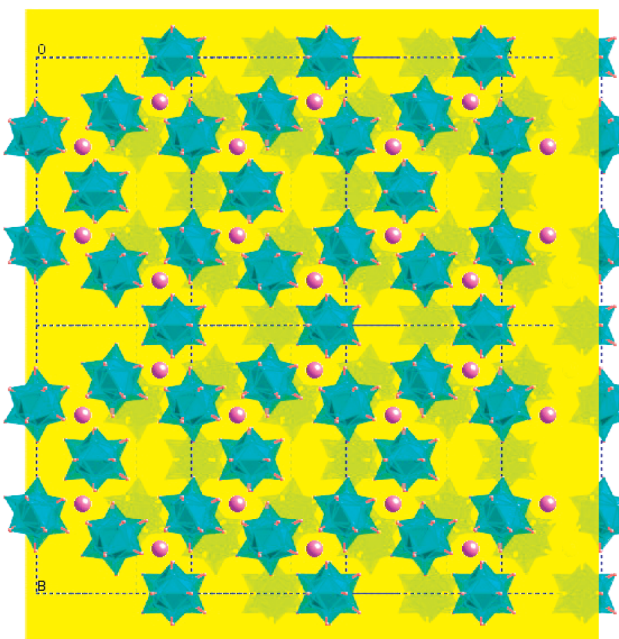
PEGS search finds a candidate ground-state crystal structure with orthorhombic C222₁ symmetry (space group No. 20), which has the lowest energy of all the considered structures (see Table 5). The C222₁ structure is 10.7 kJ/mol lower than the best ICSD structures and 44.1 kJ/mol lower than the trigonal BiI₃-type structure proposed Nakamori et al.¹⁵ Our predicted structure is shown in Figure 5 and the atomic positions are given in Table 6. The C222₁ structure has one symmetry-inequivalent type of Sc ion, two types of B ions, and 6 different H ions. Each Sc has four H ions in its nearest-neighbor coordination environment at distances of 1.91 and 2.23 Å for H5 and H6, respectively. Furthermore, each Sc has two neighboring B1 ions at a distance of 2.54 Å; these ions form zigzag...–Sc–BH₄–Sc–... chains running along the [001] direction. The...–Sc–BH₄–Sc–... chains are separated by layers of [BH₄]⁻ tetrahedra and held together

LiSc(BH₄)₄ as a Hydrogen Storage Material*J. Phys. Chem. C*, Vol. xxx, No. xx, XXXX GFigure 5. Orthorhombic *C*222₁ crystal structure of Sc(BH₄)₃.TABLE 6: Wyckoff Positions for Sc(BH₄)₃ in Space Group C222₁ (No. 20) with Lattice Parameters $a = 8.43 \text{ \AA}$, $b = 11.94 \text{ \AA}$, and $c = 7.90 \text{ \AA}$

label	type	Wyckoff position	X	Y	Z
Sc	Sc	4c	0.1882	0	0
B1	B	8c	0.3254	0.1593	0.9642
B2	B	4b	0.5	0.4978	0.25
H1	H	8c	0.4045	0.2411	0.9457
H2	H	8c	0.3191	0.0983	0.8355
H3	H	8c	0.3770	0.0950	0.0770
H4	H	8c	0.1854	0.1775	0.0036
H5	H	8c	0.1167	0.0597	0.2407
H6	H	8c	0.5192	0.4369	0.3732

496 by electrostatic interactions between negatively charged
 497 [BH₄]⁻ and positively charged Sc³⁺. The distances between
 498 Sc and out-of-plane B are 4.37 and 4.75 Å. B–H distances
 499 are predicted to vary between 1.19 Å (between B1 and H1)
 500 and 1.25 Å (B1 and H2, H3, H4). For the out-of-plane
 501 tetrahedra with B2 ions, B–H distances are all very close to
 502 1.23 Å.

503 **3. Crystal Structures of Li₂B₁₂H₁₂ and Sc₂(B₁₂H₁₂)₃**, NMR
 504 spectroscopy indicates the formation of alkali [B₁₂H₁₂]²⁻
 505 compounds such as Li₂B₁₂H₁₂ and MgB₁₂H₁₂ in the decom-
 506 position of LiBH₄ and Mg(BH₄)₂, respectively, and provides
 507 similar results in other borohydride systems.^{7,19,34} A theoretical
 508 structure of *C*2/*m* symmetry for Li₂B₁₂H₁₂ has recently been
 509 proposed based on the PEGS method.⁴³ Here, we report PEGS
 510 results for the Sc₂(B₁₂H₁₂)₃ compound, which were obtained
 511 using runs with unit cells containing one formula unit (larger
 512 unit cells are computationally very demanding, and were not
 513 attempted here). The lowest energy structure found has
 514 monoclinic *Cm* symmetry (space group No. 8) and is shown
 515 in Figure 6. This structure is built up from planes with a 2:3
 516 ratio of Sc to [BH₄]⁻ where each Sc³⁺ ion is surrounded by
 517 three [B₁₂H₁₂]²⁻ groups in a roughly symmetrical fashion;
 518 the Sc³⁺ ions form a honeycomb lattice where the [B₁₂H₁₂]²⁻
 519 groups are positioned on the edges between the Sc³⁺ ions.
 520 The successive layer are shifted relative to each other in such

Figure 6. Planar projection of the monoclinic *Cm* crystal structure of Sc₂(B₁₂H₁₂)₃. Semitransparent yellow plane marks the (001) lattice plane, Sc³⁺ ions are violet, and [B₁₂H₁₂]²⁻ groups are cyan.

521 a way that the Sc³⁺ ions are positioned on top of the
 522 [B₁₂H₁₂]²⁻ groups (see Figure 6).

523 We have not searched for the structure of a hypothetical
 524 LiSc(B₁₂H₁₂)₂ compound. While it is possible that this
 525 compound is more stable than a linear combination of
 526 Li₂B₁₂H₁₂ and Sc₂(B₁₂H₁₂)₃, we expect that the formation
 527 enthalpy will be relatively small and therefore not likely to
 528 dramatically change the main conclusions about the decom-
 529 position enthalpies and hydrogen release pathways of LiSc-
 530 (BH₄)₄.

531 **III.C. NMR Characterization of LiSc(BH₄)₄.** ¹¹B and ⁴⁵Sc
 532 MAS NMR spectra in full range of LiSc(BH₄)₄ were
 533 simulated as shown Figure 7 by using a solid-state NMR
 534 powder spectrum simulation program, QUASAR (QUAdru-
 535 polar Spectra Analysis and Refinement).⁴⁴ In these simula-
 536 tions, we considered only chemical shift anisotropy and
 537 quadrupolar interactions as major broadening sources and did
 538 not take account dipole–dipole interactions among nearby
 539 nuclei. Both spectra were well simulated while the fitting of
 540 ⁴⁵Sc MAS spectrum was not as satisfactory as the ¹¹B case.
 541 Inclusion of dipole–dipole interactions among nuclear spins
 542 (⁴⁵Sc, ¹H, ¹¹B) might be a choice for further improvement in
 543 spectral simulation, and will be a subject of future investiga-
 544 tion. From the current simulation, we obtained several NMR
 545 parameters representing information about electronic environ-
 546 ments around ¹¹B and ⁴⁵Sc nuclei which allow us to
 547 characterize the chemical bonding properties and their local
 548 structures. Chemical shift anisotropy (CSA) and quadrupolar
 549 NMR parameters are shown in Table 7. The isotropic
 550 chemical shift (δ_{iso}) of ¹¹B in the LiSc(BH₄)₄ appears between
 551 two monocation borohydrides LiBH (−41 ppm) and Sc(BH₄)₃
 552 (−18.7 ppm, in benzene-*d*₆),²⁴ certainly reflecting the change
 553 in the average Pauling electronegativity, χ_p , of the double
 554 cations. The calculated χ_p for ScLi using the equation in ref
 555 17 yielded 1.13. The quadrupolar coupling constant (C_Q) of
 556 634 kHz for ¹¹B in LiSc(BH₄)₄ is larger than those of
 557 monocation borohydrides such as LiBH₄ (105 kHz), Mg-
 558 (BH₄)₂ (~220 kHz) and Ca(BH₄)₂ (~200 kHz) which were
 559 determined in our MAS NMR experiments and QUASAR

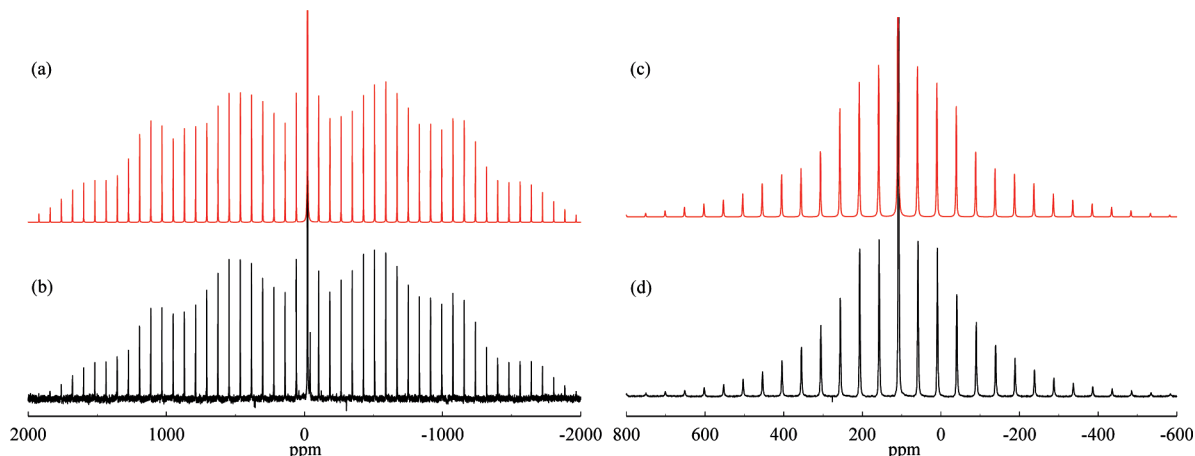


Figure 7. Simulated (a,c) and experimental (b,d) ^{11}B (a,b) and ^{45}Sc (c,d) MAS NMR spectra of the $\text{LiSc}(\text{BH}_4)_4$ compound prepared by ball milling a $4\text{LiBH}_4 + \text{ScCl}_3$ mixture.

TABLE 7: Simulated NMR Parameters of ^{11}B and ^{45}Sc of $\text{LiSc}(\text{BH}_4)_4$

nuclei	δ_{iso} (ppm)	δ_{csa} (ppm)	η_{csa}	C_Q (kHz)	η_Q
^{11}B	-22.6 ± 0.2	-49.7 ± 0.4	0.41 ± 0.06	634 ± 4	0.46 ± 0.24
^{45}Sc	108.5 ± 0.2	—	—	326 ± 11	0.8 ± 0.1

560 simulations.⁷ This difference may mean that the electron
561 distribution around ^{11}B nucleus in $\text{LiSc}(\text{BH}_4)_4$ is more
562 distorted from spherical distribution than for LiBH_4 , Mg-
563 $(\text{BH}_4)_2$, and $\text{Ca}(\text{BH}_4)_2$. The asymmetry parameter (η_Q) of
564 quadrupolar interaction of 0.5 is similar to that found⁷ for
565 LiBH_4 and the high temperature phase of $\text{Mg}(\text{BH}_4)_2$. Note
566 that the CSA of ^{45}Sc nucleus could not be determined within
567 reasonable error range from the spectra obtained in the current
568 study. Experiments at different magnetic fields are under
569 investigation to improve its contribution in ^{45}Sc MAS NMR
570 spectra. The expected ionic bonding character of double-
571 cationic $\text{LiSc}(\text{BH}_4)_4$ may account for this effect on the
572 electron distribution. Since the details in coordination
573 geometries have been explored both experimentally²¹ and
574 theoretically as in our current work, these NMR parameters
575 will be valuable resources for resolving the structural issues
576 when compared with those from the first-principles calculations.
577

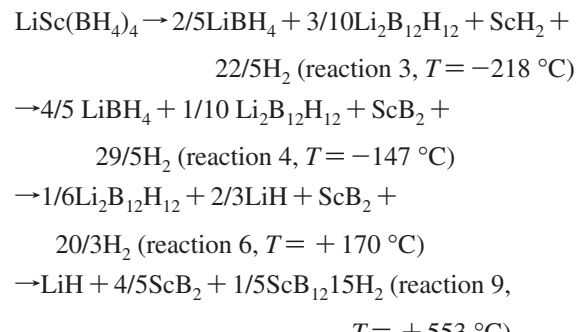
III.D. Reactivity of $\text{LiSc}(\text{BH}_4)_4$. 1. Theoretical Predictions.

578 Using the thermodynamic properties of the known Li–Sc–B–H
579 compounds listed in section III.B, PEGS-predicted crystal
580 structures of $\text{LiSc}(\text{BH}_4)_4$, $\text{Sc}(\text{BH}_4)_3$, $\text{Li}_2\text{B}_{12}\text{H}_{12}$, and Sc_2-
581 $(\text{B}_{12}\text{H}_{12})_3$, and the grand canonical linear programming
582 method,³³ we have predicted the equilibrium phase diagram
583 and hydrogen release sequence for the Li–Sc–B–H system.
584 These results are summarized in Table 8 and shown graphi-
585 cally in Figure 8. We begin by describing the stability and
586 thermodynamically preferred decomposition sequences of
587 $\text{LiSc}(\text{BH}_4)_4$ and $\text{Sc}(\text{BH}_4)_3$, followed by a full description of
588 hydrogen release pathways and thermodynamically reversible
589 hydrogen storage reactions in the Li–Sc–B–H system.

590 *Stability and Decomposition of $\text{LiSc}(\text{BH}_4)_4$.* Our calculations
591 show that $\text{LiSc}(\text{BH}_4)_4$ is thermodynamically stable against
592 decomposition into several common compounds. For the forma-
593 tion reaction, $\text{LiBH}_4 + \text{Sc}(\text{BH}_4)_3 \rightarrow \text{LiSc}(\text{BH}_4)_4$, we obtain that
594 the enthalpy change including vibrational contributions at $T =$
595 27°C is strongly negative, $\Delta H = -30 \text{ kJ/mol}$, indicating that
596 this compound should readily form upon ball-milling LiBH_4
597 and ScCl_3 . Indeed, the enthalpy difference between the reaction
598 products for the Ionic and Nonionic routes at $\text{LiBH}_4:\text{ScCl}_3$ ratios
599 of 1:4 and 1:6 in Table 1 is given by the formation enthalpy of

600 $\text{LiSc}(\text{BH}_4)_4$: negative formation enthalpy favors the Ionic route,
601 in agreement with the interpretation of our experimental NMR
602 and X-ray data given in section III.A.

603 Hydrogen release from $\text{LiSc}(\text{BH}_4)_4$ is predicted to occur via
604 a series of steps (see Table 8):



605 The equilibrium temperatures for the first two steps are very
606 low. Since hydrogen release from borohydrides typically has
607 high kinetic barriers and requires temperatures of at least a few
608 hundred $^\circ\text{C}$, it is quite likely that the first two steps will not be
609 seen until much higher temperatures due to poor kinetics. If
610 they remain “kinetically frozen” until the temperature of the
611 third step ($+170^\circ\text{C}$), the formation of LiBH_4 according to
612 reactions 3 and 4 (in Table 8) may be bypassed altogether and
613 the decomposition process may go directly into $\text{Li}_2\text{B}_{12}\text{H}_{12}$, LiH ,
614 ScB_2 , and H_2 . It is interesting to note that the overall average
615 enthalpy and entropy for the first three steps of this four-step
616 decomposition process is $\Delta H_{T=500\text{K}} = +25.4 \text{ kJ/(mol H}_2\text{)}$ and
617 $\Delta S_{T=500\text{K}} = +115 \text{ J/(mol K)}$, corresponding to a reaction that
618 becomes thermodynamically favorable at approximately -50
619 $^\circ\text{C}$, which is within the range desired for reversible on-board
620 storage. However, multistep nature of the decomposition process
621 breaks this thermodynamically attractive process into two steps
622 with enthalpies that are too low (reactions 3 and 4 in Table 8),
623 and a third step with a high enthalpy that occurs at very high
624 temperatures (reaction 6 in Table 8). If the kinetic barriers were
625 removed (e.g., by adding a suitable catalyst), only the first two
626 steps (reactions 3 and 4 in Table 8) would be observable for
627 temperatures below 80°C , and on-board rehydrogenation would
628 be difficult due to the low enthalpies of reactions 3 and 4 in
629 Table 8. Therefore, we conclude that the thermodynamics of
630 $\text{LiSc}(\text{BH}_4)_4$ are unsuitable for reversible hydrogen storage.
631

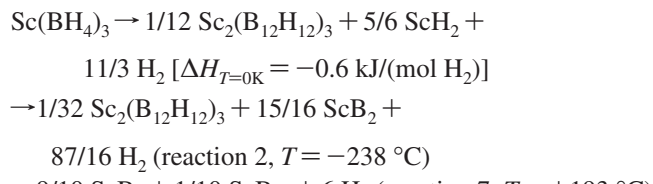
632 *Stability and Decomposition of $\text{Sc}(\text{BH}_4)_3$.* The $C222_1$ PEGS
633 structure of $\text{Sc}(\text{BH}_4)_3$ is predicted to be marginally unstable at

TABLE 8: Predicted Thermodynamically Favored Reversible Hydrogen Storage Reactions in the Li–Sc–B–H System^a

no.	reaction	wt % H ₂	T _{crit} (°C)	ΔH _{static}	ΔH _{T=0K}	ΔH _{T=500K}	ΔS _{T=500K}
1	Sc ₂ (B ₁₂ H ₁₂) ₃ + 18LiSc(BH ₄) ₄ → 9Li ₂ B ₁₂ H ₁₂ + 20ScH ₂ + 88H ₂	7.1	-257	17.5	0.3	5.8	103
2	Sc ₂ (B ₁₂ H ₁₂) ₃ + 16ScH ₂ → 18ScB ₂ + 34H ₂	5.4	-234	22.0	1.4	12.1	130
3	10LiSc(BH ₄) ₄ → 4LiBH ₄ + 3Li ₂ B ₁₂ H ₁₂ + 10ScH ₂ + 44H ₂	8.0	-218	20.4	2.8	8.5	103
4	Li ₂ B ₁₂ H ₁₂ + 5ScH ₂ → 2LiBH ₄ + 5ScB ₂ + 7H ₂	3.6	-147	32.8	9.5	22.6	142
5	2LiBH ₄ + ScH ₂ → 2LiH + ScB ₂ + 4H ₂	8.9	+44	50.6	29.2	37.1	116
6	12LiBH ₄ → Li ₂ B ₁₂ H ₁₂ + 10LiH + 13H ₂	10.0	+170	60.2	39.9	45.0	101
7	5Sc ₂ (B ₁₂ H ₁₂) ₃ + 6ScB ₂ → 16ScB ₁₂ + 90H ₂	6.1	+193	74.9	50.5	60.8	130
8	Sc ₂ (B ₁₂ H ₁₂) ₃ → 2ScB ₁₂ + 12B + 18H ₂	7.1	+214	76.7	52.5	62.5	128
9	5Li ₂ B ₁₂ H ₁₂ + 6ScB ₂ → 10LiH + 6ScB ₁₂ + 25H ₂	4.3	+553	131.5	101.4	112.7	136
10	Li ₂ B ₁₂ H ₁₂ → 2LiH + 12B + 5H ₂	6.5	+650	138.0	108.5	118.6	128

^a T_{crit} gives the hydrogen release temperature at atmospheric pressure of H₂ gas. Enthalpies are given in kJ/(mol H₂), and entropies in J/(mol K).

634 T = 0 K with respect to decomposition into Sc₂(B₁₂H₁₂)₃, ScH₂,
635 and H₂ if vibrational contributions are taken into account:



636 → 9/10 ScB₂ + 1/10 ScB₁₂ + 6 H₂ (reaction 7, T = +193 °C)

637 Again, the average of the three decomposition steps Sc(BH₄)₃
638 → (9/10)ScB₂ + (1/10)ScB₁₂ + 6H₂ has an attractive hydro-
639 genation enthalpy of ΔH_{T=500K} = +24 kJ/(mol H₂). However,
640 the formation of the [B₁₂H₁₂]⁻containing compound again breaks
641 the decomposition process into a series of steps where the first
642 two reactions have enthalpies that are too low (or are exother-
643 mic), while the last step occurs only at very high temperatures.

644 It is noteworthy that the first step of the above decomposition
645 sequence has a positive enthalpy ΔE = +19.7 kJ/(mol H₂) if
646 vibrational contributions are neglected. Therefore, static DFT
647 calculations predict that Sc(BH₄)₃ is a stable compound at T =
648 0 K. This shows the importance of vibrations in reactions
649 involving large changes in bonding environments. We refrain
650 from making definitive conclusions about the thermodynamic
651 stability of Sc(BH₄)₃ at T = 0 K due to two reasons: (1) the
652 calculated total energies contain an unknown systematic error
653 due to the approximate nature of GGA, and (2) longer PEGS
654 runs on larger-unit cell structures could further lower the
655 energies of one or both of the crystal structures of Sc(BH₄)₃
656 and Sc₂(B₁₂H₁₂)₃. Nevertheless, even if Sc(BH₄)₃ turns out to
657 be slightly stable at T = 0 K, our results suggest that the
658 hydrogen release enthalpies for the first two steps of the above
659 sequence are too low to be useful in practical on-board storage
660 systems.

661 *Phase Diagram of Li–Sc–B–H.* Figure 8 shows the calcu-
662 lated equilibrium phase diagram of the Li–Sc–B–H system
663 as a function of temperature at p = 1 bar of H₂ pressure. The
664 phase diagram is shown as a series of Gibbs triangles in the
665 space of heavy species (Li, Sc, and B) for temperature intervals
666 between successive hydrogen release reactions. The system is
667 always assumed to be in contact with a reservoir of H₂ gas at
668 p = 1 bar of H₂ pressure, so that compounds with decreasing
669 H content are formed upon increasing temperature. At T = 0
670 K, the thermodynamically stable compounds are LiH, ScH₂,
671 Sc₂(B₁₂H₁₂)₃, LiSc(BH₄)₄, Li₂B₁₂H₁₂, and LiBH₄. At each
672 temperature, the phase diagram is characterized by three kinds
673 of regions: (1) isolated points corresponding to thermodynami-
674 cally stable states where only a single phase exists (e.g., LiH,
675 ScH₂, and LiBH₄), (2) lines denoting the coexistence of two
676 phases (e.g., the line connecting LiBH₄ and LiH denotes the

677 coexistence of these two compounds), and (3) three-phase fields
678 characterized by the coexistence of the compounds at the vertices
679 defining triangular regions. As discussed above, our calculations
680 predict that Sc(BH₄)₃ is marginally unstable at T = 0 K with
681 respect to decomposition into Sc₂(B₁₂H₁₂)₃, ScH₂ and H₂; this
682 fact is reflected by the absence of Sc(BH₄)₃ in the phase diagram
683 at T = 0 K in Figure 8. However, the calculated decomposition
684 enthalpy is less than the physical accuracy of DFT, and it is
685 quite possible that Sc(BH₄)₃ is actually stable at T = 0 K and
686 metastable at room temperatures due to slow hydrogen release
687 kinetics. The first hydrogen release reaction (reaction 1 in Table
688 8) occurs for all material compositions where LiSc(BH₄)₄
689 coexists with Sc₂(B₁₂H₁₂)₃, i.e., within the two triangles defined
690 by [ScH₂, LiSc(BH₄)₄, Sc₂(B₁₂H₁₂)₃], and [Li₂B₁₂H₁₂, LiS-
691 c(BH₄)₄, Sc₂(B₁₂H₁₂)₃]. Since LiSc(BH₄)₄ and Sc₂(B₁₂H₁₂)₃ enter
692 as reactants on the left-hand side of reaction 1, this reaction
693 eliminates all fields where these phases coexist, introducing a
694 new phase-field boundary extending from ScH₂ to Li₂B₁₂H₁₂.

695 The next reaction, reaction 2 in Table 8, involves Sc₂(B₁₂H₁₂)₃
696 and ScH₂ as its products, leading to the formation of ScB₂ and
697 releasing 5.4 wt % H₂ at T = -234 °C. The reaction 2 can be
698 considered as a destabilized decomposition reaction^{8,45,46} for the
699 Sc₂(B₁₂H₁₂)₃ compound, with an enthalpy that is lowered by
700 the formation of a strongly bound ScB₂ compound on the right-
701 hand side of the reaction. LiSc(BH₄)₄ is predicted to decompose
702 according to reaction 3 in Table 8 at T = -218 °C. This leads
703 to a rearrangement of the phase diagram in Figure 8, eliminating
704 the vertex associated with LiSc(BH₄)₄ and creating a new three-
705 phase coexistence field between ScH₂, LiBH₄, and Li₂B₁₂H₁₂.
706 Even though this reaction releases a large amount of hydrogen
707 (8 wt % H₂), the thermodynamics are not compatible with
708 requirements for reversible on-board storage. At T = -147 °C,
709 we predict that reaction 4 will decompose the Li₂B₁₂H₁₂
710 compound in a destabilized reaction with ScH₂, leading to the
711 formation of ScB₂. When no ScH₂ is present, the Li₂B₁₂H₁₂
712 compound is predicted to be highly stable and decompose only
713 at very high temperatures.⁴³ The last low-temperature reaction
714 (5) involves LiBH₄ and ScH₂ as products, leading to the
715 formation of ScB₂. It is predicted to occur at T = 44 °C and
716 can be thought of as a destabilized reaction lowering the
717 decomposition enthalpy of LiBH₄ via the formation of ScB₂;
718 this reaction has been predicted previously from DFT calculations.^{47,48}
719 Even though it is predicted to release 8.9 wt % H₂, the kinetics
720 of this reaction is found to be poor.⁴⁹ Recent ¹¹B and ⁴⁵Sc NMR
721 experiments³⁴ also confirmed that ScB₂ did not form. Finally,
722 we predict that at T = +170 °C phase-pure LiBH₄ will
723 decompose into Li₂B₁₂H₁₂, LiH, and H₂ according to reaction 6
724 in Table 8. At even higher temperatures, we find a series of
725 reactions that decompose Sc₂(B₁₂H₁₂)₃ and Li₂B₁₂H₁₂; see
726 reactions 7–10 in Table 8. The corresponding changes in the

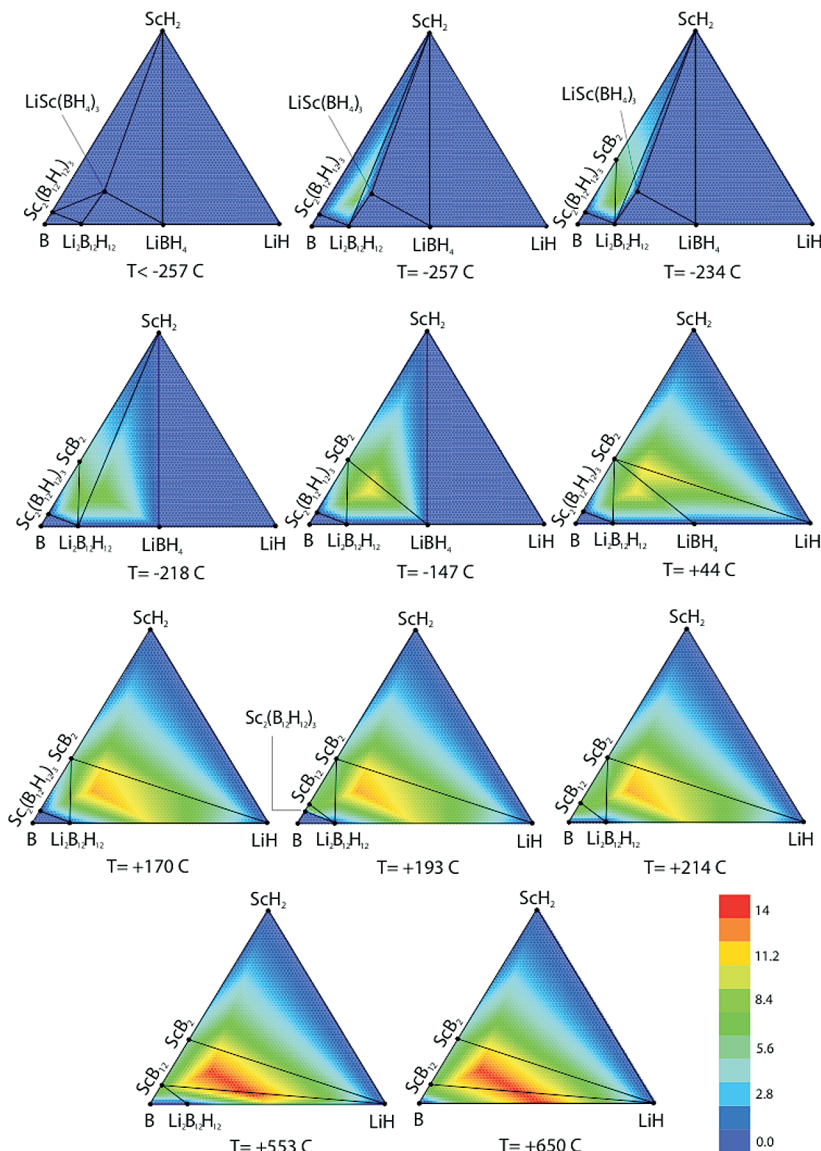


Figure 8. Calculated equilibrium phase diagram of the Li–Sc–B–H system. Color scale denotes weight percent hydrogen released relative to the starting weight of the material at $T = 0$ K.

phase diagram are shown in Figure 8. All these reactions are predicted to bind hydrogen too strongly and exhibit thermodynamics and gravimetric densities that are not useful for on-board hydrogen storage.

It is interesting that several reactions in Table 8 (reactions 1, 3, 5, and 6) have hydrogen release entropies that are significantly below the standard-state value for H_2 ($130.6 \text{ J}/(\text{mol K})$). The reasons for this behavior have been explained in ref 43. All the low-entropy reactions involve the formation of large, tightly bound $[\text{B}_{12}\text{H}_{12}]^{2-}$ groups or tightly bound bulk phases, thereby eliminating several low-frequency translational and rotational phonon branches relative to the hydrogen-rich starting compounds containing the $[\text{BH}_4]^-$ unit; this leads to higher average phonon frequencies and lower entropies in the product phases. Other things being equal, lower reaction entropies generally allow the use of materials with lower enthalpies, which are advantageous for effective heat management during on-board charging and discharging. These results show that reactions with low entropy offer another possible route for tuning reaction thermodynamics for reversible on-board storage.

2. Experimental Study of Desorption/Absorption of $\text{LiSc}(\text{BH}_4)_4$. The samples as-prepared with $n = 3, 4, 6$ in section III.A were subjected to reactivity studies similar to those used

recently on LiBH_4 and other borohydrides.^{19,34} No attempt was made to remove LiCl or LiBH_4 from the solid mixture of the product phases during these experiments. The $\text{LiSc}(\text{BH}_4)_4$ phase itself appears to be quite stable at room temperature as no noticeable changes in NMR spectra were observed after storage under argon in the glovebox for several months. The desorption behavior for each sample was performed up to maximum of 400°C in the present study. As illustrated in Figure 9 for the heated $n = 4$ sample, the XRD peaks from the initially crystalline $\text{LiSc}(\text{BH}_4)_4$ phase completely disappeared following desorption or with subsequent hydrogen absorption while the LiCl peaks sharpen slightly and shift to their reference positions. This behavior for LiCl is attributed to both particle size growth and removal of defects induced by the ball milling process. The very broad XRD peak near $2\Theta = 42^\circ$ from the desorbed and reabsorbed samples is near the maximum peak for ScB_2 , which is an expected desorption product (see above). Volumetric analyses of the hydrogen evolved during desorption indicated that losses of 5.6, 6.4, and 7.4 wt % had occurred for the $n = 3, 4$, and 6 samples, respectively. Due to the limited precision of the pressure transducers at the low pressures during these experiments, these losses have uncertainties of about ± 0.5 wt %. The predicted decrease in hydrogen from the Ionic route

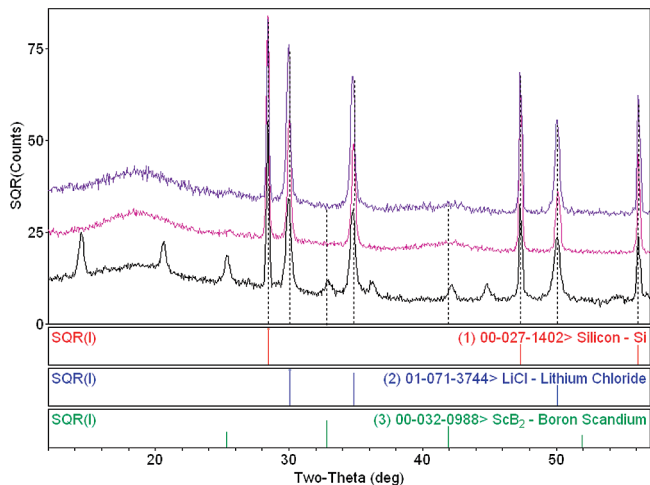
LiSc(BH₄)₄ as a Hydrogen Storage Material*J. Phys. Chem. C, Vol. xxx, No. xx, XXXX K*

Figure 9. Powder XRD profiles of as ball-milled 4LiBH₄ + ScCl₃ mixture (bottom); after a 400 °C desorption that removed about 6.4 wt % of the initial hydrogen content (middle); and following a 400 °C desorption and a subsequent hydrogen absorption under ~70 bar of H₂ gas and cooling to room temperature (top).

products given in Table 1 are respectively 5.2, 6.3, and 7.5 wt % for this series where complete desorption results in formation of LiH, ScB₂, and B from the borohydride phases. Hence, the reasonable agreement with experiment indicated that nearly all of the desorbable hydrogen was removed. The loss of hydrogen contents from the desorbed samples was also apparent from the decreases in the ¹H MAS NMR spectra (~95% of ¹H signal) when compared to signal from as-prepared samples (spectra not shown). However, accurate quantitative evaluation was not accessible by ¹H NMR due to severe probe detuning from these neat samples that is associated with formation of metallic compounds such as ScB₂. The powders collected from the desorption reactor had to be diluted by mixing with dehydrated quartz powder (SiO₂) for NMR measurements, which impacted reliability of determining proton contents. While sample spinning and probe detuning problem were resolved with the dilution method, we typically observe significant line broadening in MAS NMR spectra, causing difficulties in access of phase identification and nearly impractical quantitative analysis. All these line broadenings indicate that the desorbed products were in amorphous phases, which has been discussed more thoroughly in previous papers.^{7,19} The complete absence of XRD peaks from the desorbed samples as shown in Figure 9 is entirely consistent with these amorphous phases. Our discussion in this section, therefore, is limited to addressing identifiable major components in amorphous phases. Figure 10 showed ¹¹B and ⁴⁵Sc MAS NMR spectra of the desorbed Sc–Li–B–H systems that are compared to reference spectra. These ¹¹B spectra indicated that ScB₂ was the apparent major product in the 3:1 ratio sample, but as the mixing ratio increased the amount of ScB₂ formation decreased while the amount of [B₁₂H₁₂]²⁻ phase (i.e., Li form) formed increased. Note additional broadening and shifting of ScB₂ peak position in ¹¹B MAS NMR toward to the upfield as the mixing ratio increases. Besides the ScB₂ peak at ~90 ppm, an additional boron signal was found to be present as a broad line between 0 and 100 ppm for all three samples. Its presence is rather clearly revealed in ¹¹B MQMAS spectrum (see Supporting Information, Figure S1-a)) as a narrow strip along the isotropic chemical shift axis, a typical NMR signature of amorphous phase.¹⁹ While a part of the signal could be associated with elemental boron in amorphous phase (~5 ppm with line width (fwhm) ~ 35 ppm),¹⁹ scandium borides species

like in ScB₁₂ (see above and Table 8) could possibly explain the NMR peak. However, our current speculation on its identity needs further investigation. The similar unusual behavior was observed for ⁴⁵Sc MAS NMR and the broadening gets to be so severe that the phase identification by NMR becomes inconclusive. It is likely that ⁴⁵Sc MAS NMR spectra in Figure 10 showed both ScB₂ and ScH₂ species formed during the decomposition reaction. Less ScB₂ appeared to be produced while the ScH₂ formation was relatively increased during the desorption reaction as the mixing ratio (i.e., LiBH₄ to ScCl₃) of the ball-milled reactants increased. The result is consistent with higher amount of Li₂B₁₂H₁₂ observed in ¹¹B MAS NMR spectra in Figure 10 for samples with higher *n* values, demonstrating that the ScB₂ formation is a result of a reaction between Li₂B₁₂H₁₂ and ScH₂ as our theoretical study predicted (see above, reaction 4 in Table 8). The poor conversion to ScB₂ observed especially for the 1:6 sample is believed to be associated with the presence of excess LiBH₄. The excess LiBH₄ could interfere with reaction equilibrium of LiSc(BH₄)₄ decomposition (see Table 8).

In summary for LiSc(BH₄)₄ desorption experiment, we have observed formation of ScB₂, B, and residual amounts of LiBH₄, Li₂B₁₂H₁₂ via MAS NMR detection. Although the volumetric data had suggested nearly complete removal of hydrogen during the 400 °C desorptions, the NMR results clearly show decomposition was not complete. In fact, we found previously^{19,34} that temperatures exceeding 500–550 °C are usually needed to remove the B₁₂H₁₂-containing phases. The formation of Sc₂(B₁₂H₁₂)₃ could not be addressed in our current study. As pointed above, from the competition between thermodynamics and kinetics, the decomposition of the LiSc(BH₄)₄ phase could easily be inhomogeneous with variable amounts of ScB₂ and Li₂B₁₂H₁₂ depending upon the presence of excess LiBH₄ where most LiBH₄ more readily¹⁹ decomposed into Li₂B₁₂H₁₂. Any reversibility of these reactions could be dependent on both the composition and factors such as heating rate and hydrogen overpressure during desorption.^{8,9} A systematic exploration in desorption behavior LiSc(BH₄)₄ at lower reaction temperatures appears to be required for further understanding of the compound.

Reabsorption of hydrogen by desorbed LiSc(BH₄)₄ was examined using the desorbed [4LiBH₄ + ScCl₃] material. Figures 11 and 12 show the ¹¹B and ⁴⁵Sc MAS NMR spectra of this desorbed and reabsorbed sample, respectively. From the ¹¹B NMR spectra most of boron species including ScB₂ and B formed during desorption had changed into Li₂B₁₂H₁₂ with only a small amount of LiBH₄ compound being regenerated. This observation suggests that Li₂B₁₂H₁₂ is the most stable compound with retention of residual amounts of hydrogen during both desorption and absorption reactions. In order to recover fully the hydrogen-rich compound such as LiBH₄ from the desorbed boron materials, hydrogen pressure much greater than 70 bar appear to be required.³⁴ Note that use of 2D MQMAS NMR method (see Supporting Information, Figure S1-b) allowed us to identify the presence of residual B and the broad boron signal (0–100 ppm, see above) while the presence of ScB₂ was not confirmed in any case. The ⁴⁵Sc NMR peak for ScB₂ compound was not detected as well (not shown in Figure 12). A new Sc-containing compound associated with the peak at 150 ppm in Figure 12b was formed after the reabsorption treatment instead of LiSc(BH₄)₄ and ScCl₃. This compound is not fully identified at the moment. Although in the literature the tetragonal structure of LiScO₂ was reported⁵⁰ to be 148 ppm and 1.6 MHz for quadrupole coupling constant, it is unlikely to consider its appearance as an absorption product. Oxide contamination to

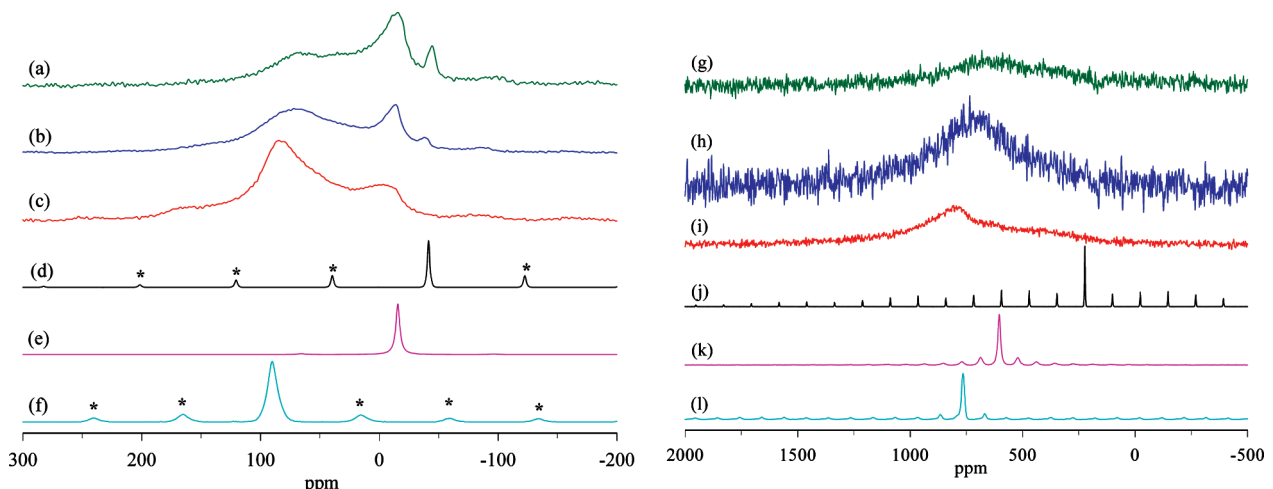


Figure 10. ^{11}B (a–f) and ^{45}Sc (g–l) MAS NMR spectra of the desorbed $\text{ScCl}_3 + n\text{LiBH}_4$: (a,g) $n = 6$, (b,h) $n = 4$, (c,i) $n = 3$, and (d) LiBH_4 , (e) $\text{Li}_2\text{B}_{12}\text{H}_{12}$, (f,l) ScB_2 , (j) ScCl_3 , (k) ScH_2 . The asterisks in (d,f) indicate spinning sidebands. All the peaks except for the highest ones in (j–l) are also spinning sidebands.

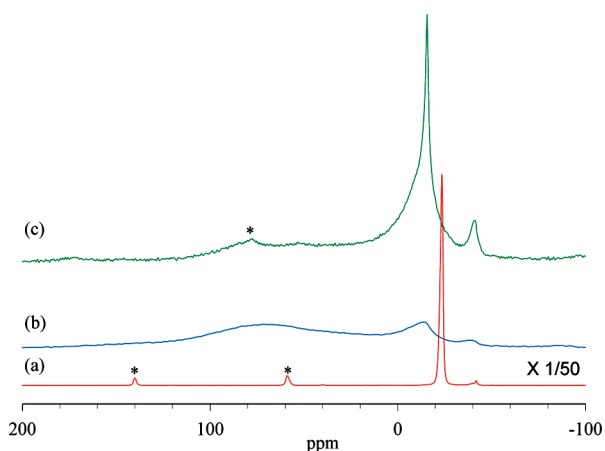


Figure 11. ^{11}B MAS NMR spectra of (a) as-made, (b) desorbed, and (c) reabsorbed $\text{ScCl}_3 + 4\text{LiBH}_4$. The asterisks indicate spinning sidebands.

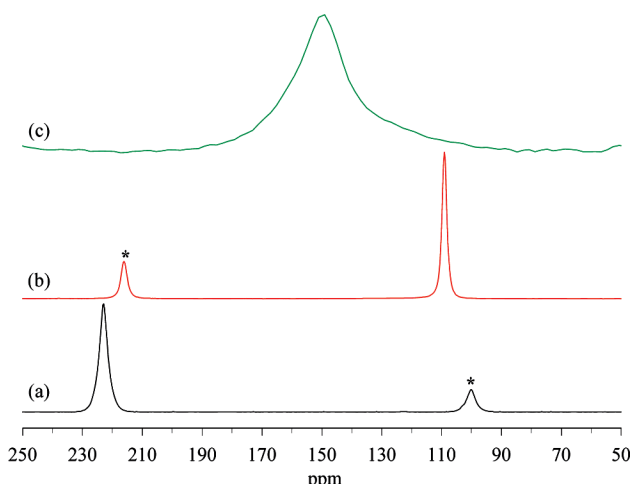


Figure 12. ^{45}Sc MAS NMR spectra of (a) ScCl_3 (Aldrich), (b) as-made $\text{LiSc}(\text{BH}_4)_4$, and (c) reabsorbed $\text{ScCl}_3 + 4\text{LiBH}_4$. The asterisks indicate spinning sidebands.

boron species is not detected in ^{11}B MAS NMR. We believe that identification of this scandium compound should play a key role in understanding the transformation of ScB_2 upon hydrogenation. Most LiCl formed in the ball-milling process remained crystalline and not participating in any reaction during

the reabsorption as confirmed by ^6Li MAS NMR studies (not shown). In summary, reabsorption at 400 °C and hydrogen pressure of 70 bar results in small reconversion of hydrogen-rich boron compounds $\text{Li}_2\text{B}_{12}\text{H}_{12}$ and LiBH_4 . Regeneration of $\text{LiSc}(\text{BH}_4)_4$ was not detected.

IV. Conclusions

The reaction products in Li–Sc–B–H systems have been investigated by the combination of the multinuclear solid-state NMR, powder XRD, and first-principles calculation methods. The solid-phase reaction during the ball milling of $\text{ScCl}_3 + n\text{LiBH}_4$ was demonstrated to occur via the ionic route leading to the formation of $\text{LiSc}(\text{BH}_4)_4$ rather than the nonionic route that would result in the formation of $\text{Sc}(\text{BH}_4)_3$. Only $\text{LiSc}(\text{BH}_4)_4$ was synthesized by the ball-milling process instead of $\text{Sc}(\text{BH}_4)_3$, which is in complete agreement with our first-principles calculations of relative stabilities. This ternary borohydride compound showed more than 99% loss of hydrogen during gas desorption under the mild desorption condition. The identified desorption products were mainly the ScB_2 , B, ScH_2 , and $\text{Li}_2\text{B}_{12}\text{H}_{12}$ compounds. The reabsorption in Li–Sc–B–H system results in the formation of $\text{Li}_2\text{B}_{12}\text{H}_{12}$ as a major product along with some increase in the LiBH_4 content. The reaction mechanism and chemical products in the mechanical ball milling, desorption, and reabsorption process of the complex borohydride system could be identified by using high-resolution solid-state NMR techniques.

Acknowledgment. We thank Dr. Channing Ahn for his contributions and support. This research was partially performed at the Jet Propulsion Laboratory, which is operated by the California Institute of Technology under contract with the NASA. This work was partially supported by DOE through Award Nos. DE-AI-01-05EE11105, DE-FC36-05GO15065, and DE-FC36-05GO15062. The NMR facility at Caltech was supported by the National Science Foundation (NSF) under Grant No. 9724240 and partially supported by the MRSEC Program of the NSF under Award No. DMR-0520565. Research at UCLA was supported by the U.S. Department of Energy under grant No. DE-FG02-07ER46433 and by the DOE INCITE program. Research at UMSL was funded by the U.S. Department of Energy, Office of Energy Efficiency and Renewable Energy, in the Hydrogen, Fuel Cells & Infrastructure Technologies Program under Contract No. DE-AC04-94AL8500.

LiSc(BH₄)₄ as a Hydrogen Storage Material

Supporting Information Available: ¹¹B 2D multiple-quantum (MQ) MAS spectra for ScCl₃ + 4LiBH₄ mixture desorbed at 400 °C and after absorption of at 400 °C and at 70 bar of H₂. This material is available free of charge via the Internet at <http://pubs.acs.org>.

References and Notes

- (1) Züttel, A.; Borgschulte, A.; Orimo, S.-I. *Scr. Mater.* **2007**, *56*, 823.
 (2) Orimo, S.-I.; Nakamori, Y.; Eliseo, J. R.; Züttel, A.; Jensen, C. M. *Chem. Rev.* **2007**, *107*, 4111.
 (3) Satyapal, S.; Petrovic, J.; Read, C.; Thomas, G.; Ordaz, G. *Catal. Today* **2007**, *120*, 246.
 (4) Jeon, E.; Cho, Y. *J. Alloys Compd.* **2006**, *422*, 273.
 (5) Au, M.; Jurgensen, A. R.; Spencer, W. A.; Anton, D. L.; Pinkerton, F. E.; Hwang, S.-J.; Kim, C.; Bowman, R. C. *J. Phys. Chem. C* **2008**, *112*, 18661.
 (6) Züttel, A.; Wenger, P.; Rentsch, S.; Sudan, P.; Mauron, P.; Emmenegger, C. *J. Power Sources* **2003**, *118*, 1.
 (7) Soloveichik, G. L.; Gao, Y.; Rijssenbeek, J.; Andrus, M.; Krajanski, S.; Bowman Jr, R. C.; Hwang, S.-J.; Zhao, J.-C. *Int. J. Hydrogen Energy* **2009**, *34*, 916.
 (8) Vajo, J. J.; Skeith, S. L.; Mertens, F. *J. Phys. Chem. B* **2005**, *109*, 3719.
 (9) Pinkerton, F. E.; Meyer, M. S.; Meisner, G. P.; Balogh, M. P.; Vajo, J. J. *J. Phys. Chem. C* **2007**, *111*, 12881.
 (10) Kostka, J.; Lohstroh, W.; Fichtner, M.; Hahn, H. *J. Phys. Chem. C* **2007**, *111*, 14026.
 (11) Wan, X.; Markmaitree, T.; Osborn, W.; Shaw, L. L. *J. Phys. Chem. C* **2008**, *112*, 18232.
 (12) Vajo, J. J.; Olson, G. L. *Scr. Mater.* **2007**, *56*, 829.
 (13) Gross, A. F.; Vajo, J. J.; Van Atta, S. L.; Olson, G. L. *J. Phys. Chem. C* **2008**, *112*, 5651.
 (14) Yu, X. B.; Wu, Z.; Chen, Q. R.; Li, Z. L.; Weng, B. C.; Huang, T. S. *Appl. Phys. Lett.* **2007**, *90*, 034106.
 (15) Nakamori, Y.; Miwa, K.; Ninomiya, A.; Li, H.; Ohba, N.; Towata, S.-i.; Züttel, A.; Orimo, S.-i. *Phys. Rev. B (Condens. Matter Mater. Phys.)* **2006**, *74*, 045126.
 (16) Nakamori, Y.; Li, H. W.; Kikuchi, K.; Aoki, M.; Miwa, K.; Towata, S.; Orimo, S. *J. Alloys Compd.* **2007**, *446–447*, 296.
 (17) Li, H. W.; Orimo, S.; Nakamori, Y.; Miwa, K.; Ohba, N.; Towata, S.; Züttel, A. *J. Alloys Compd.* **2007**, *446–447*, 315.
 (18) Nakamori, Y.; Li, H. W.; Matsu, M.; Miwa, K.; Towata, S.; Orimo, S. *J. Phys. Chem. Solids* **2008**, *69*, 2292.
 (19) Hwang, S.-J.; Bowman, R. C.; Reiter, J. W.; Rijssenbeek, J.; Soloveichik, G. L.; Zhao, J.-C.; Kabbour, H.; Ahn, C. C. *J. Phys. Chem. C* **2008**, *112*, 3164.
 (20) Bowman, R. C., Jr.; Reiter, J. W.; Hwang, S.-J.; Kim, C.; Kabbour, H. In *Materials Issues in a Hydrogen Economy*; Jena, P., Kandalam, A., Sun, Q., Eds.; in press, 2009.
 (21) Hagemann, H.; Longhini, M.; Kaminski, J. W.; Wesolowski, T. A.; Cerny, R.; Penin, N.; Sorby, M. H.; Hauback, B. C.; Severa, G.; Jensen, C. M. *J. Phys. Chem. A* **2008**, *112*, 7551.
 (22) Lobkovskii, É. B.; Kravchenko, S. E.; Semenenko, K. N. *J. Struct. Chem.* **1977**, *18*, 312.
 (23) Morris, J. H.; Smith, W. E. *J. Chem. Soc. D* **1970**, 245a.
 (24) Mancini, M.; Bougeard, P.; Burns, R. C.; Mlekuz, M.; Sayer, B. G.; Thompson, J. I. A.; McGlinchey, M. J. *Inorg. Chem.* **1984**, *23*, 1072.
 (25) Kresse, G.; Furthmüller, J. *Comput. Mater. Sci.* **1996**, *6*, 15.
 (26) Kresse, G.; Furthmüller, J. *Phys. Rev. B* **1996**, *54*, 11169.
 (27) Perdew, J. P.; Wang, Y. *Phys. Rev. B* **1992**, *45*, 13244.
 (28) Perdew, J. P.; Burke, K.; Ernzerhof, M. *Phys. Rev. Lett.* **1996**, *77*, 3865.
 (29) Kresse, G.; Joubert, D. *Phys. Rev. B* **1999**, *59*, 1758.
 (30) Blöchl, P. E. *Phys. Rev. B* **1994**, *50*, 17953.
 (31) Wolverton, C.; Ozolins, V.; Asta, M. *Phys. Rev. B* **2004**, *69*, 144109.
 (32) Majzoub, E. H.; Ozolins, V. *Phys. Rev. B (Condens. Matter Mater. Phys.)* **2008**, *77*, 104115.
 (33) Akbarzadeh, A. R.; Ozolins, V.; Wolverton, C. *Adv. Mater.* **2007**, *19*, 3233.
 (34) Purewal, J.; Hwang, S.-J.; Bowman, J.; Robert, C.; RoInnebro, E.; Fultz, B.; Ahn, C. *J. Phys. Chem. C* **2008**, *112*, 8481.
 (35) Bennett, A. E.; Rienstra, C. M.; Auger, M.; Lakshmi, K. V.; Griffin, R. G. *J. Chem. Phys.* **1995**, *103*, 6951.
 (36) Amoureaux, J.-P.; Pruski, M. *Mol. Phys.* **2002**, *100*, 1595.
 (37) Mali, G.; Kaucic, V. *J. Chem. Phys.* **2002**, *117*, 3327.
 (38) Bohnsack, A.; Stenzel, F.; Zajonc, A.; Balzer, G.; Wickleder, M. S.; Meyer, G. Z. *Anorg. Allg. Chem.* **1997**, *623*, 1067.
 (39) Lu, J.; Fang, Z. Z.; Sohn, H. Y.; Bowman, R. C.; Hwang, S.-J. *J. Phys. Chem. C* **2007**, *111*, 16686.
 (40) Vidal, J. P.; Vidal-Valat, G. *Acta Crystallogr. B* **1986**, *42*, 131.
 (41) Khodyrev, Y. P.; Baranova, R. V. *Kristallografiya* **1980**, *25*, 172.
 (42) Majzoub, E. H.; RoInnebro, E. *J. Phys. Chem. C* **2009**, *113*, 3352.
 (43) Ozolins, V.; Majzoub, E. H.; Wolverton, C. *J. Am. Chem. Soc.* **2009**, *131*, 230.
 (44) Amoureaux, J. P.; Fernandez, C.; Carpenterier, L.; Cochon, E. *Phys. Status Solidi (a)* **1992**, *132*, 461.
 (45) Reilly, J. J.; Wiswall, R. H. *Inorg. Chem.* **1967**, *6*, 2220.
 (46) Reilly, J. J.; Wiswall, R. H. *Inorg. Chem.* **1968**, *7*, 2254.
 (47) Alapati, S. V.; Johnson, J. K.; Sholl, D. S. *J. Phys. Chem. C* **2008**, *112*, 5258.
 (48) Siegel, D. J.; Wolverton, C.; Ozolins, V. *Phys. Rev. B (Condens. Matter Mater. Phys.)* **2007**, *76*, 134102.
 (49) Yang, J.; Sudik, A.; Wolverton, C. *J. Phys. Chem. C* **2007**, *111*, 19134.
 (50) Kim, N.; Hsieh, C.-H.; Stebbins, J. F. *Chem. Mater.* **2006**, *18*, 3855.

JP9011685